

Consecutive topological transitions of helical Fermi arcs at saddle points in CoSi

Zhicheng Rao^{1,2†}, Shangjie Tian^{3†}, Shunye Gao^{1,2}, Quanxin Hu^{1,2}, Wenhui Fan^{1,2},
Jierui Huang^{1,2}, Cenyao Tang^{1,2}, Yaobo Huang⁴, Hechang Lei^{3*}, Yujie Sun^{1,7*},
Tian Qian^{1,5*}, and Hong Ding^{1,5,6}

¹ Beijing National Laboratory for Condensed Matter Physics and Institute of Physics, Chinese Academy of Sciences, Beijing 100190, China;

² University of Chinese Academy of Sciences, Beijing 100049, China;

³ Department of Physics and Beijing Key Laboratory of Opto-electronic Functional Materials & Micro-nano Devices, Renmin University of China, Beijing 100872, China;

⁴ Shanghai Synchrotron Radiation Facility, Shanghai Advanced Research Institute, Chinese Academy of Sciences, Shanghai 201210, China;

⁵ Songshan Lake Materials Laboratory, Dongguan 523808, China;

⁶ CAS Center for Excellence in Topological Quantum Computation, University of Chinese Academy of Sciences, Beijing 100190, China;

⁷ Department of Physics, South University of Science and Technology, Shenzhen 518055, China

Received November 8, 2021; accepted January 27, 2022; published online March 29, 2022

The CoSi family hosts unconventional topological nodes with nonzero Chern numbers. The nontrivial topology is manifested by conspicuous surface Fermi arcs connecting surface projections of the nodes. Here, using angle-resolved photoemission spectroscopy, we have systematically investigated the (001) surface states of pristine and Ni-doped CoSi. The surface states form saddle-like band structures at/near the time-reversal invariant point near the Fermi level. The Fermi arcs undergo consecutive Lifshitz transitions at the saddle points \bar{X} , leading to changes of the Fermi arc configuration. As the density of states has a van Hove singularity at the saddle points, exotic many-body physical phenomena may emerge accompanied by the topological transitions of surface Fermi arcs.

topological transition, Fermi arcs, saddle point

PACS number(s): 73.20.At, 68.37.-d, 03.65.Vf

Citation: Z. Rao, S. Tian, S. Gao, Q. Hu, W. Fan, J. Huang, C. Tang, Y. Huang, H. Lei, Y. Sun, T. Qian, and H. Ding, Consecutive topological transitions of helical Fermi arcs at saddle points in CoSi, *Sci. China-Phys. Mech. Astron.* **65**, 257013 (2022), <https://doi.org/10.1007/s11433-021-1867-y>

1 Introduction

The nontrivial topology in materials is manifested by protected electronic states on the boundary due to the bulk-boundary correspondence. In three-dimensional (3D) topological semimetals, when a band-crossing nodal point carries

a nonzero Chern number (C), such as the well-known Weyl nodes ($C = \pm 1$), its surface projection is surrounded by surface states with a helical band structure [1-5]. The helical surface states are two-dimensional (2D) analogy of the chiral edge states of integer quantum Hall insulators. The constant-energy contours of helical surface states are open Fermi arcs, which connect the surface projections of a pair of topological nodes with opposite chirality, i.e., the sign of Chern numbers [1-5], as illustrated in Figure 1(e). The Fermi arcs have been

*Corresponding authors (Tian Qian, email: tqian@iphy.ac.cn; Yujie Sun, email: sunyj@sustech.edu.cn; Hechang Lei, email: hlei@ruc.edu.cn)

†These authors contributed equally to this work.

observed in a range of Weyl semimetals, such as the TaAs family [6-11], (Mo,W)Te₂ [12-14], and Co₃Sn₂S₂ [15,16], as well as the CoSi family [17-21], which has topological nodes with higher Chern numbers, in angle-resolved photoemission spectroscopy (ARPES) experiments. The Fermi arcs not only play a key role in experimental identification of topological semimetals, but also result in many unusual physical properties, such as periodic-in-1/B quantum oscillations in density of states (DOS) [22,23], 3D quantum Hall effect [24,25], and chiral magnetic effects [26,27].

So far, these behaviors related to the Fermi arcs have been well understood in the framework of non-interacting fermions. On the other hand, many-body interactions in condensed matter systems also give rise to many fascinating phenomena, such as unconventional superconductivity, Mott insulators, and charge density wave (CDW). While superconductivity, CDW, and magnetic order have been found in the bulk of many topological materials, many-body effects on the topological surface states have remained elusive for a long time. Very recently, we have observed an incommensurate CDW persisting even up to room temperature on the (001) surface of CoSi, which was attributed to many-body interactions associated with the Fermi arcs [28]. The intriguing behavior inspires us to systematically investigate the (001) surface states of pristine and Ni-doped CoSi single crystals. Our ARPES results reveal that the helical surface states on the (001) surface of CoSi form multiple saddle points, at which the Fermi arcs undergo consecutive topological transitions. Since electron correla-

tions are significantly enhanced at the saddle points, it is expected to uncover more physical phenomena induced by many-body interactions in the topological surface states.

2 Methods

High-quality single crystals of pristine and Ni-doped CoSi were grown by the chemical vapor transport method. ARPES measurements were carried out at the “Dreamline” beamline of the Shanghai Synchrotron Radiation Facility with a Scienta Omicron DA30L analyzer. To obtain atomically flat surfaces for the ARPES measurements, we polished the (001) surface of single crystals, and then repeatedly sputtered the surfaces and annealed the samples until clear reflection high-energy electron diffraction patterns appeared [29].

3 Results and discussion

CoSi crystalizes in space group $P2_13$ (No. 198) with chiral cubic lattices, which have no mirror, inversion, and roto-inversion symmetries. Figure 1(b) shows that when spin-orbit coupling (SOC) is not included, the band structure near the Fermi level (E_F) has three- and four-fold degenerate nodal points at Γ and R, respectively. The calculations have indicated that the nodes carry nonzero Chern numbers ± 2 without SOC [30-33]. On the (001) surface, the two nodes at Γ and R are projected to the surface Brillouin zone (BZ)

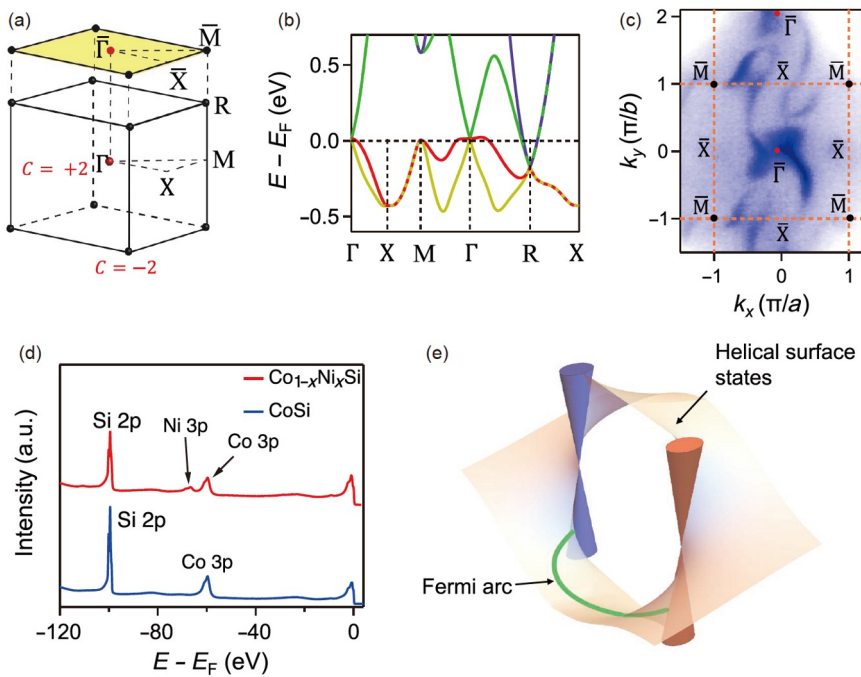


Figure 1 (Color online) Nontrivial topological properties in CoSi. (a) Bulk BZ and (001) surface BZ of CoSi. (b) Calculated bulk band structure along high-symmetry lines without SOC. (c) ARPES intensity map at E_F measured with $h\nu = 110$ eV on the (001) surface of CoSi. (d) Core-level photoemission spectra of pristine and Ni-doped CoSi samples. (e) Schematic of helical surface states near the projections of a pair of Weyl nodes with opposite chirality.

center Γ and corner \bar{M} , respectively (Figure 1(a)). Two Fermi arcs emanate from the projection of each node on the (001) surface corresponding to $C = \pm 2$. When SOC is included, because of the lack of inversion symmetry, finite spin splitting is induced in all surface bands and most bulk bands, and the nodes at Γ and R carry Chern numbers ± 4 [31,32]. Four Fermi arcs emanate from the projection of each node on the (001) surface corresponding to $C = \pm 4$. However, owing to the weak SOC strength in CoSi, the splitting in both bulk and surface bands is too small to be resolved in the ARPES experiments. Therefore, we discuss the experimental results under the framework without SOC.

Figure 1(c) shows the ARPES intensity map at E_F measured at photon energy $h\nu = 110$ eV. Our previous study has indicated that most ARPES spectra detected with vacuum ultraviolet light come from the surface states of CoSi because of the short mean free path of excited photoelectrons [17]. The intensity map exhibits that two Fermi arcs emanate from $\bar{\Gamma}$, diagonally cross the surface BZ, and end at \bar{M} , corresponding to $C = \pm 2$ without SOC. At the (001) surface, almost all lattice symmetries in the bulk are broken, and only in-plane translation symmetry and time-reversal symmetry are preserved. The Fermi arcs are related by π rotation with respect to the time-reversal invariant points Γ , \bar{M} , or X ,

which is constrained by time-reversal symmetry [33].

We first investigate the helical surface states in the vicinity of Γ and \bar{M} . We have performed ARPES measurements on CoSi samples at 195 K. The Fermi-Dirac distribution function is broadened at finite temperatures, resulting in partial occupation within a few $k_B T$ above E_F . Therefore, the ARPES experiments at 195 K can detect the electronic states within tens of meV above E_F . Figure 2(b) and (c) show the ARPES intensity maps at different constant energies around Γ and \bar{M} . The Fermi arcs almost connect to Γ , whereas they do not reach \bar{M} since the node at \bar{M} is enclosed by projected Fermi surfaces (FSs) of bulk states. The Fermi arcs at different energy levels are plotted together in Figure 2(d) and (e). With raising the energy, the Fermi arcs rotate clockwise and anticlockwise with respect to Γ and \bar{M} , respectively. Figure 2(f) and (g) show surface band dispersions on the loops encircling Γ and \bar{M} , respectively. There are two parallel bands on each loop, but the bands between the two loops have opposite signs of velocity, which is dictated by opposite Chern numbers of the nodes at Γ and R. We combine the Fermi arcs and surface bands in Figure 2(h) and (i). It is clear that the rotation of Fermi arcs with energy arises from the helical surface states around surface projections of the nodes.

As seen in Figure 3(a), since two ends of the Fermi arcs

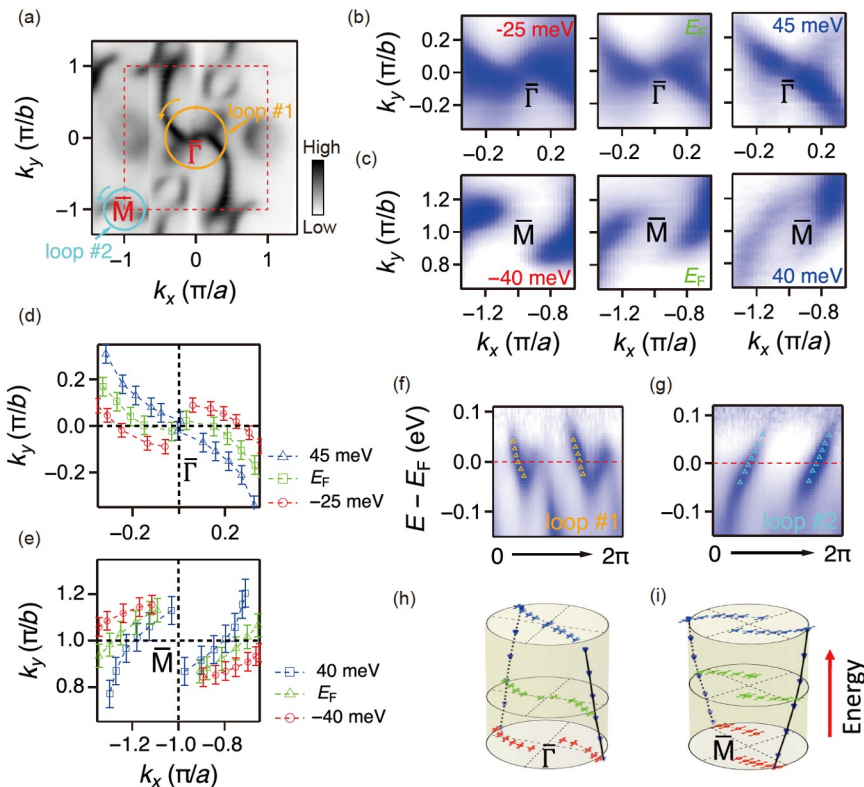


Figure 2 (Color online) Helical surface bands and Fermi arcs around Γ and \bar{M} . (a) ARPES intensity map at E_F measured with $h\nu = 55$ eV. (b) ARPES intensity maps at -25 meV (left), E_F (middle), and 45 meV (right) around Γ . (c) ARPES intensity maps at -40 meV (left), E_F (middle), and 40 meV (right) around \bar{M} . (d), (e) Fermi arcs extracted from the data in (b) and (c), respectively. ARPES intensity plots showing surface band dispersions along loops #1 (f) and #2 (g), whose momentum locations are indicated as orange and cyan circles in (a). 3D plots of the extracted Fermi arcs and surface bands around Γ (h) and \bar{M} (i).

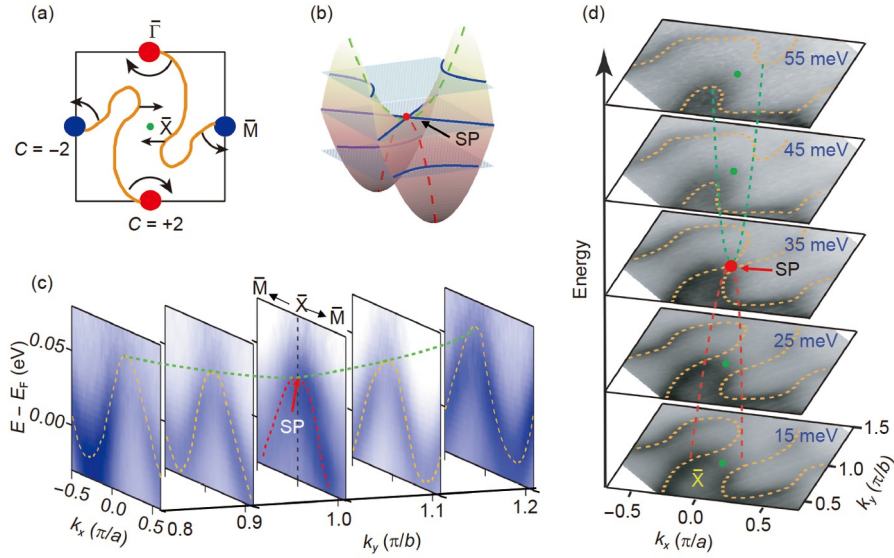


Figure 3 (Color online) Saddle point of the surface states at \bar{X} . (a) Fermi arcs at E_F on the (001) surface of CoSi. The arrows indicate the moving directions of the Fermi arcs with raising the energy. (b) Schematic of the saddle-like band structure. SP is the abbreviation of saddle point. (c) ARPES intensity plots showing the saddle-like band dispersions near \bar{X} . (d) ARPES intensity maps around \bar{X} at 15, 25, 35, 45, and 55 meV, showing that the Fermi arcs undergo a Lifshitz transition at 35 meV. Red and green dashed lines are guide to eyes for the band dispersions below and above the saddle point, respectively.

rotate clockwise and anticlockwise, respectively, the middle part of the Fermi arcs will stretch toward the \bar{X} point with energy shift. Figure 3(d) shows evolution of the Fermi arcs around \bar{X} above E_F . With raising the energy, the two Fermi arcs first approach gradually, touch each other at \bar{X} at 35 meV, and separate again at higher energies. The evolution of Fermi arcs with energy indicates that the surface states form a saddle point at 35 meV above E_F at \bar{X} , as illustrated in Figure 3(b). To further illuminate the saddle point, we plot surface band dispersions near \bar{X} in Figure 3(c), which exhibit hole-like bands along the k_x direction below the saddle point but electron-like bands along the k_y direction above the saddle point. These results demonstrate that the helical surface states form a saddle point at the time-reversal invariant point \bar{X} , at which the Fermi arcs undergo a Lifshitz transition.

Figure 4(a)-(f) exhibit that the Lifshitz transition significantly changes the topological configuration of Fermi arcs in CoSi. For convenience, we divide \bar{M} into \bar{M}_1 and \bar{M}_2 and \bar{X} into \bar{X}_1 and \bar{X}_2 in the surface BZ, as indicated in Figure 4(a). Figure 4(a)-(d) show that when the energy levels lie below the saddle point at 35 meV, the Fermi arcs keep connecting between Γ and \bar{M}_1 . When the energy level rises above the saddle point, the Fermi arc configuration switches to the connection between Γ and \bar{M}_2 in Figure 4(e) and (f).

As the energy level continues to rise, we observe another Lifshitz transition near \bar{X}_2 , which results in the Fermi arc configuration switching again. The Fermi arcs gradually approach the FS surrounding \bar{X}_2 with raising the energy, as

marked with red arrows in Figure 4(d)-(f). We estimate that the Fermi arcs would touch the FS at ~ 80 meV above E_F in CoSi. However, owing to the limitation of the Fermi-Dirac distribution function, the band structures at higher energies cannot be detected in pristine CoSi samples. Therefore, we have performed ARPES measurements on $\text{Co}_{1-x}\text{Ni}_x\text{Si}$ samples, whose chemical potential is elevated by electron doping, allowing us to investigate the band structures at higher energies. Figure 4(g)-(i) show the constant-energy maps of $\text{Co}_{1-x}\text{Ni}_x\text{Si}$ at -170 meV, -85 meV and E_F , respectively. The Fermi arcs almost touch the FS at \bar{X}_2 in Figure 4(g), while the Fermi arcs and FS combine into new Fermi arcs in Figure 4(h). The Fermi arcs undergo another Lifshitz transition between Figure 4(g) and (h). Likewise, the Lifshitz transition occurs at a saddle point, at which the Fermi arc touches the FS at \bar{X}_2 . The Lifshitz transition results in the Fermi arc configuration switching to the connection between Γ and \bar{M}_1 , as seen in Figure 4(g) and (h).

We plot three representative contours of surface states at different energy levels in Figure 4(j), where the Fermi arcs stretch along $\bar{M}_1\Gamma\bar{M}_1$, $\bar{M}_2\Gamma\bar{M}_2$, and $\bar{M}_1\Gamma\bar{M}_1$ in sequence. To illustrate the topological transition of Fermi arcs, we draw a schematic plot of combined surface states of two pairs of topological nodes in Figure 5(a). The interplay of the helical surface states generates a saddle-like band structure. The Fermi arcs meet when sweeping the energy through the saddle point, resulting in a Lifshitz transition, whereas they are less affected near the nodes. As a result, the Fermi arc configuration is changed through the saddle point. Based on the scenario, we summarize the evolution of the Fermi arc

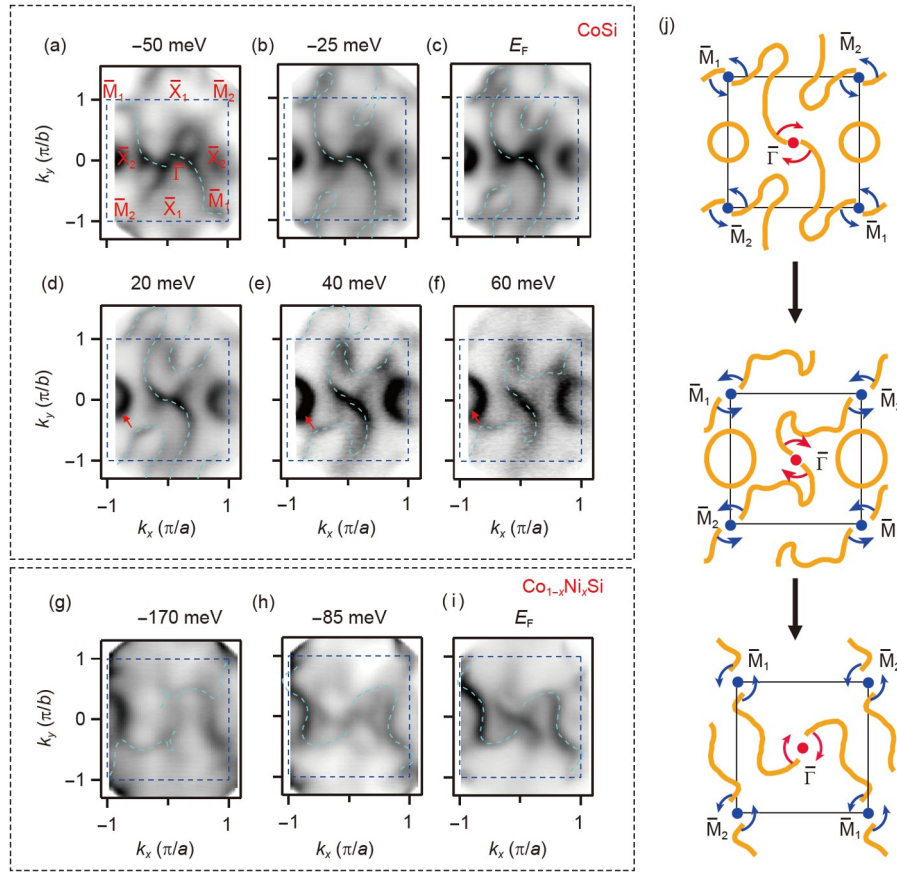


Figure 4 (Color online) Lifshitz transitions of helical Fermi arcs in CoSi and $\text{Co}_{1-x}\text{Ni}_x\text{Si}$. (a)-(f) ARPES intensity maps at -50, -25, 0, 20, 40, and 60 meV at 196 K in CoSi. Cyan dashed lines are guide to eyes for the Fermi arcs. (g)-(i) ARPES intensity maps at -170 meV, -85 meV and E_F at 30 K in Ni-doped CoSi. (j) Extracted Fermi arcs at E_F (top) and 60 meV (middle) in CoSi and at E_F (bottom) in Ni-doped CoSi.

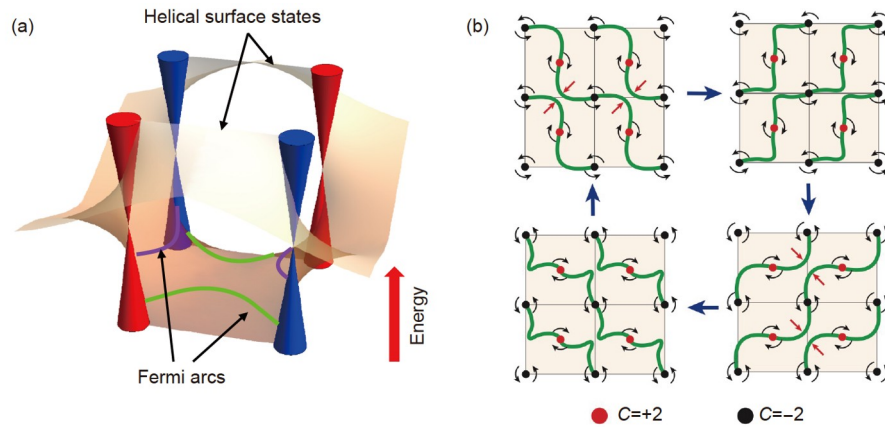


Figure 5 (Color online) Consecutive topological transitions of helical Fermi arcs. (a) Schematic of combined helical surface states of two pairs of topological nodes. Purple and green lines represent the Fermi arcs lying above and below a saddle point, respectively. (b) Schematics of the evolution of Fermi arcs with sweeping the energy in CoSi, illustrating consecutive topological transitions of helical Fermi arcs at saddle points. Arrows between the schematics refer to the upward energy shift.

configuration with energy in CoSi in Figure 5(b). For simplicity, we ignore the FS at \bar{X}_2 , which arises from local distortion of the surface band structures. The helical surface

states form saddle points at the \bar{X} point. The Fermi arcs rotate continuously with sweeping the energy. When the Fermi arcs meet at the saddle points, a Lifshitz transition occurs, re-

sulting in a switch of the topological configuration of the Fermi arcs. The configuration is restored when it switches twice with sweeping the energy, forming a closed loop as shown in Figure 5(b). The topological transitions occur repeatedly until the projected FSs of the nodes expand to connect with each other.

4 Conclusion

Our results have revealed that the helical surface states on the (001) surface of CoSi form multiple saddle points, at which the Fermi arcs undergo topological transitions. At a saddle point of band dispersions in 2D systems, the density of states has a van Hove singularity of logarithmic divergency. The chemical potential of CoSi can be easily tuned via element substitution. When the saddle points approach E_F , the increased density of states enhances electron correlations, which would lead to various instabilities, such as superconductivity [34], magnetism [35], and charge/spin density wave [36,37]. As the CDW instability has been observed in the topological surface states of CoSi, it is promising to uncover more fascinating phenomena induced by electron correlations by finely tuning the chemical potential of the surface states in the future.

We thank Tiantian Zhang and Chen Fang for enlightening discussions. This work was supported by the Ministry of Science and Technology of China (Grant Nos. 2016YFA0401000, 2016YFA0300600, 2018YFE0202600, and 2016YFA0300504), the National Natural Science Foundation of China (Grant Nos. U1832202, 11774423, 118224121, and 1888101), the Chinese Academy of Sciences (Grant Nos. QYZDB-SSW-SLH043, XDB33020100, and XDB28000000), the Beijing Natural Science Foundation (Grant No. Z200005), the Fundamental Research Funds for the Central Universities and Research Funds of Renmin University of China (Grant Nos. 18XNLG14, and 19XNLG17), and the Beijing Municipal Science and Technology Commission (Grant No. Z171100002017018). Yaobo Huang acknowledges support by the CAS Pioneer “Hundred Talents Program” (type C).

- 1 X. Wan, A. M. Turner, A. Vishwanath, and S. Y. Savrasov, *Phys. Rev. B* **83**, 205101 (2011), arXiv: 1007.0016.
- 2 G. Xu, H. Weng, Z. Wang, X. Dai, and Z. Fang, *Phys. Rev. Lett.* **107**, 186806 (2011), arXiv: 1106.3125.
- 3 H. Weng, C. Fang, Z. Fang, B. A. Bernevig, and X. Dai, *Phys. Rev. X* **5**, 011029 (2015), arXiv: 1501.00060.
- 4 S. M. Huang, S. Y. Xu, I. Belopolski, C. C. Lee, G. Chang, B. K. Wang, N. Alidoust, G. Bian, M. Neupane, C. Zhang, S. Jia, A. Bansil, H. Lin, and M. Z. Hasan, *Nat. Commun.* **6**, 7373 (2015).
- 5 C. Fang, L. Lu, J. Liu, and L. Fu, *Nat. Phys.* **12**, 936 (2016), arXiv: 1512.01552.
- 6 B. Q. Lv, H. M. Weng, B. B. Fu, X. P. Wang, H. Miao, J. Ma, P. Richard, X. C. Huang, L. X. Zhao, G. F. Chen, Z. Fang, X. Dai, T. Qian, and H. Ding, *Phys. Rev. X* **5**, 031013 (2015), arXiv: 1502.04684.
- 7 S. Y. Xu, I. Belopolski, N. Alidoust, M. Neupane, G. Bian, C. Zhang, R. Sankar, G. Chang, Z. Yuan, C. C. Lee, S. M. Huang, H. Zheng, J. Ma, D. S. Sanchez, B. K. Wang, A. Bansil, F. Chou, P. P. Shibayev, H. Lin, S. Jia, and M. Z. Hasan, *Science* **349**, 613 (2015), arXiv: 1502.03807.
- 8 B. Q. Lv, N. Xu, H. M. Weng, J. Z. Ma, P. Richard, X. C. Huang, L. X. Zhao, G. F. Chen, C. E. Matt, F. Bisti, V. N. Strocov, J. Mesot, Z. Fang, X. Dai, T. Qian, M. Shi, and H. Ding, *Nat. Phys.* **11**, 724 (2015), arXiv: 1503.09188.
- 9 L. X. Yang, Z. K. Liu, Y. Sun, H. Peng, H. F. Yang, T. Zhang, B. Zhou, Y. Zhang, Y. F. Guo, M. Rahn, D. Prabhakaran, Z. Hussain, S. K. Mo, C. Felser, B. Yan, and Y. L. Chen, *Nat. Phys.* **11**, 728 (2015).
- 10 S. Y. Xu, N. Alidoust, I. Belopolski, Z. Yuan, G. Bian, T. R. Chang, H. Zheng, V. N. Strocov, D. S. Sanchez, G. Chang, C. Zhang, D. Mou, Y. Wu, L. Huang, C. C. Lee, S. M. Huang, B. K. Wang, A. Bansil, H. T. Jeng, T. Neupert, A. Kaminski, H. Lin, S. Jia, and M. Zahid Hasan, *Nat. Phys.* **11**, 748 (2015).
- 11 D. F. Xu, Y. P. Du, Z. Wang, Y. P. Li, X. H. Niu, Q. Yao, P. Dudin, Z. A. Xu, X. G. Wan, and D. L. Feng, *Chin. Phys. Lett.* **32**, 107101 (2015), arXiv: 1509.03847.
- 12 K. Deng, G. Wan, P. Deng, K. Zhang, S. Ding, E. Wang, M. Yan, H. Huang, H. Zhang, Z. Xu, J. Denlinger, A. Fedorov, H. Yang, W. Duan, H. Yao, Y. Wu, S. Fan, H. Zhang, X. Chen, and S. Zhou, *Nat. Phys.* **12**, 1105 (2016), arXiv: 1603.08508.
- 13 L. Huang, T. M. McCormick, M. Ochi, Z. Zhao, M. T. Suzuki, R. Arita, Y. Wu, D. Mou, H. Cao, J. Yan, N. Trivedi, and A. Kaminski, *Nat. Mater.* **15**, 1155 (2016), arXiv: 1603.06482.
- 14 J. Jiang, Z. K. Liu, Y. Sun, H. F. Yang, C. R. Rajamathi, Y. P. Qi, L. X. Yang, C. Chen, H. Peng, C. C. Hwang, S. Z. Sun, S. K. Mo, I. Vobornik, J. Fujii, S. S. P. Parkin, C. Felser, B. H. Yan, and Y. L. Chen, *Nat. Commun.* **8**, 13973 (2017), arXiv: 1604.00139.
- 15 D. F. Liu, A. J. Liang, E. K. Liu, Q. N. Xu, Y. W. Li, C. Chen, D. Pei, W. J. Shi, S. K. Mo, P. Dudin, T. Kim, C. Cacho, G. Li, Y. Sun, L. X. Yang, Z. K. Liu, S. S. P. Parkin, C. Felser, and Y. L. Chen, *Science* **365**, 1282 (2019), arXiv: 1909.09580.
- 16 Q. Wang, Y. Xu, R. Lou, Z. Liu, M. Li, Y. Huang, D. Shen, H. Weng, S. Wang, and H. Lei, *Nat. Commun.* **9**, 3681 (2018), arXiv: 1712.09947.
- 17 Z. Rao, H. Li, T. Zhang, S. Tian, C. Li, B. Fu, C. Tang, L. Wang, Z. Li, W. Fan, J. Li, Y. Huang, Z. Liu, Y. Long, C. Fang, H. Weng, Y. Shi, H. Lei, Y. Sun, T. Qian, and H. Ding, *Nature* **567**, 496 (2019).
- 18 D. S. Sanchez, I. Belopolski, T. A. Cochran, X. Xu, J. X. Yin, G. Chang, W. Xie, K. Manna, V. Süß, C. Y. Huang, N. Alidoust, D. Multer, S. S. Zhang, N. Shumiya, X. Wang, G. Q. Wang, T. R. Chang, C. Felser, S. Y. Xu, S. Jia, H. Lin, and M. Z. Hasan, *Nature* **567**, 500 (2019).
- 19 D. Takane, Z. Wang, S. Souma, K. Nakayama, T. Nakamura, H. Oinuma, Y. Nakata, H. Iwasawa, C. Cacho, T. Kim, K. Horiba, H. Kumigashira, T. Takahashi, Y. Ando, and T. Sato, *Phys. Rev. Lett.* **122**, 076402 (2019), arXiv: 1809.01312.
- 20 N. B. M. Schröter, D. Pei, M. G. Vergniory, Y. Sun, K. Manna, F. de Juan, J. A. Krieger, V. Süss, M. Schmidt, P. Dudin, B. Bradlyn, T. K. Kim, T. Schmitt, C. Cacho, C. Felser, V. N. Strocov, and Y. Chen, *Nat. Phys.* **15**, 759 (2019), arXiv: 1812.03310.
- 21 H. Li, S. Xu, Z. C. Rao, L. Q. Zhou, Z. J. Wang, S. M. Zhou, S. J. Tian, S. Y. Gao, J. J. Li, Y. B. Huang, H. C. Lei, H. M. Weng, Y. J. Sun, T. L. Xia, T. Qian, and H. Ding, *Nat. Commun.* **10**, 5505 (2019), arXiv: 1912.02383.
- 22 A. C. Potter, I. Kimchi, and A. Vishwanath, *Nat. Commun.* **5**, 5161 (2014), arXiv: 1402.6342.
- 23 D. Bulmash, and X. L. Qi, *Phys. Rev. B* **93**, 081103 (2016), arXiv: 1512.03437.
- 24 C. M. Wang, H. P. Sun, H. Z. Lu, and X. C. Xie, *Phys. Rev. Lett.* **119**, 136806 (2017), arXiv: 1705.07403.
- 25 C. Zhang, Y. Zhang, X. Yuan, S. Lu, J. Zhang, A. Narayan, Y. Liu, H. Zhang, Z. Ni, R. Liu, E. S. Choi, A. Suslov, S. Sanvito, L. Pi, H. Z. Lu, A. C. Potter, and F. Xiu, *Nature* **565**, 331 (2019).
- 26 S. Zhong, J. E. Moore, and I. Souza, *Phys. Rev. Lett.* **116**, 077201 (2016), arXiv: 1510.02167.
- 27 C. K. Chan, P. A. Lee, K. S. Burch, J. H. Han, and Y. Ran, *Phys. Rev. Lett.* **116**, 026805 (2016), arXiv: 1509.05400.

- 28 Z. C. Rao, Q. X. Hu, S. J. Tian, S. Y. Gao, Z. Y. Yuan, C. Y. Tang, W. H. Fan, J. R. Huang, Y. B. Huang, L. Wang, L. Zhang, F. S. Li, H. X. Yang, H. M. Weng, T. Qian, J. P. Xu, K. Jiang, H. C. Lei, Y. J. Sun, and H. Ding, arXiv: [2110.07815](https://arxiv.org/abs/2110.07815).
- 29 C. Y. Tang, Z. C. Rao, Q. Q. Yuan, S. J. Tian, H. Li, Y. B. Huang, H. C. Lei, S. C. Li, T. Qian, Y. J. Sun, and H. Ding, *Chin. Phys. B* **29**, 028101 (2020).
- 30 B. Bradlyn, J. Cano, Z. Wang, M. G. Vergniory, C. Felser, R. J. Cava, and B. A. Bernevig, *Science* **353**, aaf5037 (2016).
- 31 G. Chang, S. Y. Xu, B. J. Wieder, D. S. Sanchez, S. M. Huang, I. Belopolski, T. R. Chang, S. Zhang, A. Bansil, H. Lin, and M. Z. Hasan, *Phys. Rev. Lett.* **119**, 206401 (2017).
- 32 P. Tang, Q. Zhou, and S. C. Zhang, *Phys. Rev. Lett.* **119**, 206402 (2017), arXiv: [1706.03817](https://arxiv.org/abs/1706.03817).
- 33 T. Zhang, Z. Song, A. Alexandradinata, H. Weng, C. Fang, L. Lu, and Z. Fang, *Phys. Rev. Lett.* **120**, 016401 (2018), arXiv: [1705.07244](https://arxiv.org/abs/1705.07244).
- 34 M. L. Kiesel, C. Platt, W. Hanke, D. A. Abanin, and R. Thomale, *Phys. Rev. B* **86**, 020507 (2011), arXiv: [1109.2953](https://arxiv.org/abs/1109.2953).
- 35 M. Fleck, A. M. Oleś, and L. Hedin, *Phys. Rev. B* **56**, 3159 (1997), arXiv: [cond-mat/9911367](https://arxiv.org/abs/cond-mat/9911367).
- 36 D. Makogon, R. van Gelderen, R. Roldán, and C. M. Smith, *Phys. Rev. B* **84**, 125404 (2011), arXiv: [1104.5334](https://arxiv.org/abs/1104.5334).
- 37 C. Honerkamp, *Phys. Rev. Lett.* **100**, 146404 (2008), arXiv: [0711.1259](https://arxiv.org/abs/0711.1259).